Host CD59 Potentiates the Type III Secretion System in *Yersinia pseudotuberculosis*

Kristen J. Davis[1,2,#], Kerri-Lynn Sheahan[1,3,*], Connor S. Murphy[1,3,*] and Ralph R. Isberg[1,3]

[1]Department of Molecular Biology and Microbiology

[2]Graduate Program in Molecular Microbiology, Tufts University Graduate School of Biomedical Sciences

[3]Tufts University School of Medicine, Boston, MA, USA

Running title: CD59 contributes to T3SS Function in *Y. pseudotuberculosis*

Keywords: *Yersinia*/CD59/Focal Adhesions/Type III Secretion/Lipids

[#]Address correspondence to Ralph.Isberg@tufts.edu

[*]Present addresses: Kerri Sheahan, Obsidian Therapeutics;

Connor Murphy, Graduate School of Biomedical Sciences and Engineering, University of Maine

Abstract

Type III secretion systems (T3SS) play critical roles in disease for many Gram-negative pathogens. For *Yersinia pseudotuberculosis* (*Yptb*), the machinery delivers the Yop bacterial effectors into host cells, misregulating cytoskeletal components and sabotaging immune defenses. Although the structural details of T3SS assembly have been extensively studied, the intimate interactions between T3SS components and the target host plasma membrane are poorly characterized. A previous RNA interference (RNAi) study identified the GPI-linked surface protein CD59 as a critical host component that supports T3SS translocation pore formation and effector movement into the host cytosol. We show here that both depletion and increased levels of CD59 reduced *Yptb* T3SS pore formation and Yop translocation into host target cells. Enzymatic removal of all GPI-linked surface proteins from wild-type cells prior to *Yptb* infection had no effect on T3SS function, indicating that neither CD59 nor other GPI-linked proteins were receptors for the T3SS machinery. Consistent with its importance in supporting the T3SS function, efficient bacterial effector-mediated focal adhesion disassembly was dependent on CD59. Depletion of CD59 interfered with the rearrangement of the lipid raft marker GM1 that occurs after *Yptb* adhesion to host cells, indicating that CD59 supports lipid microdomain dynamics. Consistent with a role in modulating lipid composition, the loss of CD59 resulted in the accumulation of phosphatidylcholine lipids and alterations in both fatty acid chain lengths and fatty acid saturation levels. This work points to a role for CD59 in supporting efficient T3SS function by maintaining plasma membrane dynamics necessary to support efficient T3SS function.

41

42 **Introduction**

43 The pathogenesis of *Yersinia pseudotuberculosis* (*Yptb*) requires the Type III Secretion
44 System (T3SS), which delivers bacterial effectors into host cells, thereby misregulating host
45 signaling pathways and facilitating evasion of innate immune responses (1-3). The T3SS is
46 encoded on a ~70-kb virulence plasmid present in the three human-pathogenic *Yersinia* species:
47 the enteropathogenic *Y. enterocolitica* and *Y. pseudotuberculosis*, and the causative agent of
48 bubonic plague, *Y. pestis* (4-6). The secretion apparatus is structurally and functionally well
49 conserved among many Gram-negative pathogens, with the *Yersinia* syringe-like nanomachine
50 delivering bacterial effector proteins, called Yops (*Yersinia* outer proteins), into the host cell
51 cytosol (2, 7). There is a core set of six Yops, with YopT absent in most *Yptb* strains (including
52 YPIII, the strain used in this study) (8, 9). Although much work has been done to describe the
53 structure and function of the T3SS, how the host cell supports its function remains largely
54 unknown.

55 Yops prevent engulfment by professional phagocytes and interfere with reactive oxygen-
56 mediated killing, allowing successful extracellular bacterial replication and survival in host
57 tissues, even with neutrophil-adherent bacteria (3, 10). YopE, for example, is a GTPase
58 activating protein (GAP) that inactivates Rho-family GTPases such as RhoA, Cdc42, and Rac
59 that regulate actin cytoskeletal function required for phagocytosis and production of reactive
60 oxygen species via assembly of the NADPH oxidase complex (11, 12). Interestingly, it has been
61 shown that host cell Rho GTPase activity is initially required for efficient translocation of Yops
62 (13), underscoring that modulation of the actin cytoskeleton plays multiple roles in establishing
63 disease. Several other host factors have been identified that are important for T3SS function,

64 including host cell sulfation and fucosylation in *Vibrio parahaemolyticus*, and DNAJC5 in
65 *Pseudomonas aeruginosa*, which acts as a chaperone for effector translocation (14-16).
66 We previously identified mammalian proteins important for YopE function using a
67 mammalian siRNA knockdown library and a FRET-based Rho GTPase biosensor (17). The
68 screen identified host proteins, including the chemokine receptor CCR5, which has been shown
69 to affect T3SS function, as well as other proteins involved in cell adhesion, signaling, and
70 membrane trafficking (17). These included CD59, a glycosyl-phosphatidylinositol (GPI)-
71 anchored protein on the surface of most mammalian cell types that functions as a self-recognition
72 marker to protect against complement attack (18). The presence of CD59 on mammalian cells
73 prevents the oligomerization of complement proteins into membrane attack complexes (MACs)
74 upon activation, whereas microorganisms lacking this defense are targeted for destruction (19-
75 21). CD59 is also a direct receptor for some bacterial cholesterol-dependent pore-forming
76 cytolysins and may play a role in forming the T3SS translocation channel (22, 23). In addition,
77 CD59 is an important component of microdomains in the plasma membrane, known as lipid
78 rafts, which are important for critical cell functions such as membrane trafficking, chemokine
79 signaling, and immune cell activation (24). Studies in several similar pathogens, including
80 *Shigella*, EPEC, and *Salmonella,* have revealed that functional lipid rafts on the host cell surface
81 play an important role in supporting microbial adhesion, T3SS translocon pore insertion, and
82 delivery of translocated effector substrates (25-27).
83 In this study, we show that cells lacking CD59 are associated with aberrant mobilization
84 of host cell plasma membrane components in response to *Yptb*-target cell contact, resulting in
85 defective translocon pore formation and effector translocation.
86

87 **Results**

88 **Alterations in surface expression of host cell CD59 result in inefficient pore formation by**
89 ***Yptb***

90 The plasma membrane protein CD59 was identified as a candidate for supporting Yop
91 translocation, based on a pooled shRNA knockdown approach to detect mammalian proteins
92 important for *Yptb* YopE function (17). Verification of the hit revealed that when host cell CD59
93 was knocked down by shRNA, significant T3SS defects were evident, as assessed by secondary
94 assays for YopB/D-dependent pore formation and YopH translocation (17). These data were
95 consistent with a general defect in T3SS translocator function rather than direct modulation of
96 YopE activity. To pursue these results further, a cloned CD59 knockout HEK 293T line (CD59
97 KO) was constructed (28). Cell surface labeling of the CD59 KO cell line with anti-CD59-FITC,
98 followed by flow cytometry analysis, resulted in fluorescence indistinguishable from that of an
99 isotype control (Figure 1A). In contrast, WT HEK 293T cells, showed robust labeling with the
100 anti-CD59-FITC conjugate (Figure 1A).

101 To determine if *Yptb* challenge of the CD59 KO cell line exhibited translocation defects
102 similar to those observed in the shRNA knockdown, a T3SS pore formation assay was
103 performed. Once injected into a target cell, the Yop effectors downmodulate pore formation to
104 prevent immediate cytotoxicity of the host (29). Therefore, a Δ*yopHMOJE* (YPIIIΔ5) strain that
105 lacks all regulatory Yops and exhibits hyper pore-forming activity was used to measure pore
106 formation, measuring fluorescence of an amine-reactive membrane-impermeant probe as a proxy
107 (17).

108 The *Yersinia* translocon pore complex comprises the two hydrophobic pore proteins
109 YopB and YopD, along with the hydrophilic scaffolding protein LcrV, which localizes to the

110 needle tip (7). A *yopB* mutant strain (YPIIIΔB), lacking the major translocon pore protein YopB,
111 is unable to form pores in the host cell plasma membrane and serves as a negative control for
112 pore formation and translocation (10). WT and CD59 KO cells were challenged with YPIIIΔB or
113 YPIIIΔB at MOI = 25 for 2 hours and analyzed for FITC incorporation by flow cytometry. WT
114 and CD59 KO cells infected with the YPIIIΔB mutant were intact and unperturbed, as shown by
115 their similarly low background fluorescence (Figure 1B). In WT cells infected with YPIII□5,
116 two distinct right-shifted populations labeled by the probe were observed. The peak furthest to
117 the right indicates maximum cytotoxicity, while the wider, shouldered peak represents varying
118 degrees of pore formation. The CD59 KO cells also showed these two populations, but there was
119 a distinct leftward shift toward lower probe incorporation, indicating that cells lacking CD59
120 were less susceptible to pore formation by YPIIIΔB than WT cells (Figure 1B).
121 To further interrogate the effect of CD59 plasma membrane levels on *Yptb* T3SS function,
122 WT CD59 was introduced into the CD59 KO cell line to evaluate if pore-forming activity could
123 be restored. Human CD59 expressed from the mammalian expression vector pcDNA3.1+ was
124 transfected into CD59 KO 293T cells, and monoclonal populations were isolated after antibiotic
125 selection. Two clones exhibiting CD59 levels similar to WT (KOpCD59-WT1 and KOpCD59-
126 WT2), as well as two clones with increased surface levels of CD59 (KOpCD59-OE1 and
127 KOpCD59-OE2) were identified (Figure 1C). Each of these clones, along with the WT and KO
128 cell lines, was assayed for pore formation after infection by YPIIIΔ5. Interestingly, both CD59
129 clones with increased surface levels of CD59 showed similar resistance to pore formation by
130 YPIIIΔ5 compared to what was observed with the KO cells. The only clone that restored the
131 degree of pore formation seen in WT cells was one of the clones that exhibited WT levels of
132 surface CD59 (Figure 1D; WT1). Although clones could be isolated that restored pore formation

133 by YPIIIΔ5, there appeared to be confounding effects that prevented effective complementation.
134 In addition to the clones shown here, random screening of several clones that overproduced
135 CD59 relative to WT failed to show the same level of pore formation as the WT1 clone (Figure
136 1D).

137 Phenotypic variation was observed among the CD59 KO and KOpCD59 clones after
138 prolonged passaging, introducing another confounding factor. Strategies were sought to
139 overcome this issue. CD59 is one of the most abundant GPI-linked proteins, so knocking it out
140 may select for suppressor mutations or unpredictable changes in regulatory patterns that could be
141 propagated over many passages. For this reason, we continued investigating the role of CD59 in
142 *Yptb* T3SS function using transient siRNA knockdown. Efficient CD59 knockdown was
143 achieved 72 hours post-transfection using mixed pools of siRNAs directed against CD59
144 (Materials and Methods; Figure 2A).

145 To evaluate siCD59 knockdown populations using a strategy that does not require loss of
146 membrane integrity or causing cell lethality, T3SS function was assessed by measuring Yop
147 translocation into host cells, detected by assaying for YopE-TEM (or YPIIIΔB YopE-TEM)
148 translocation using a β-lactamase reporter strain followed by FACS analysis (30). After a 1hr
149 infection at MOI = 1, HEK 293T cells were loaded with CCF4-AM, a FRET-based β-lactamase
150 substrate that readily enters the host cells as detected by a green fluorescence signal at 515nm
151 after 409nm excitation. Translocation of YopE-TEM was detected by cleavage of the TEM
152 substrate which results in a blue fluorescence signal at 450nm using the same excitation
153 wavelength, visualizing translocation by the fluorescence intensity of 450nm emission relative to
154 515nm emission after 409nm excitation. This was displayed with contour plots of the blue vs.
155 green channels (Figure 2B). Green cells were gated with the YPIIIΔB YopE-TEM negative

156 control (Figure 2B, left panel). After a 1hr infection of siNT cells with YopE-TEM,
157 approximately 65% of the gated blue vs. green cells shifted to the blue gate, indicating robust
158 translocation (Figure 2B, middle panel). In the siCD59 infection (Figure 2B, right panel) this was
159 reduced to 45% of the gated cells, with no detectable translocation in almost 32% of the cells.
160 The total translocation in the population was reduced by about 50% as well, based on the ratio of
161 the total fluorescence intensity at 450nm to 515nm in siCD59 knockdown cells from triplicate
162 samples (Figure 2C).
163
164 **Host cell CD59 indirectly supports *Yptb* T3SS-dependent pore formation**
165 Intermedilysin (ILY) is a bacterial-encoded cholesterol-dependent pore-forming toxin
166 (PFT) from *Streptococcus intermedius* that requires CD59 as a receptor (22). The wild-type form
167 of this protein (ILY^{WT}) forms pores in the host cell membrane, whereas a mutant version that is
168 fixed in a prepore conformation (ILY^{PP}) binds CD59 without forming an active pore, leaving the
169 host cell membrane intact (31). The *Yptb* translocon pore proteins YopB and YopD share
170 physiological properties with PFTs (32), and we hypothesized that if the *Yptb* translocon pore
171 interacts with CD59 similarly to ILY, then ILY^{PP} binding to CD59 will block T3SS-dependent
172 pore formation.
173 His-ILY^{WT} and His-ILY^{PP} were expressed in *E. coli* BL21 (DE3) and purified (Materials
174 and Methods). HEK 293T cells were pretreated with ILY^{PP} or mock buffer, challenged with
175 ILY^{WT}, and assayed for pore formation. Cells that were mock-treated and challenged with ILY^{WT}
176 exhibited high levels of pore formation, confirming that the ILY^{WT} was functioning properly
177 (Figure 3A). Cells pretreated with ILY^{PP} were protected from pore formation, indicating that the
178 mutant protein successfully bound the CD59 receptor and blocked ILY^{WT} (Figure 3A). To

179 determine if ILY^{PP} could block *Yptb* T3SS-dependent pore formation, 293T cells were pretreated
180 with ILY^{PP} for 1 hour and then challenged with YPIIIΔ5 or YPIIIΔB at MOI = 25 for 2 hours
181 (Figure 3B). There was no difference in pore formation among the ILY^{PP} pretreated and mock-
182 treated cells, indicating that if there was a direct interaction between CD59 and the T3SS
183 machinery, it did not occur at the ILY binding site.

184 To eliminate the possibility that an insufficient quantity of ILY^{PP} was added to the cells to
185 block all binding sites, cells were treated with phospholipase C (PLC), an enzyme that cleaves
186 above the phosphoinositol group of the GPI-anchor, releasing CD59 and other GPI-linked
187 proteins. WT 293T cells were pretreated with PLC, challenged with YPIIIΔ5, then assayed for
188 pore formation. This strategy depleted GPI-linked proteins based on detection of these linkages
189 with Alexa488-conjugated proaerolysin, as PLC treatment resulted in a distinct decrease in
190 fluorescence compared to the mock-treated cell population (Figure 3C). After the 2 hr infection
191 with YPIIIΔ5, there was no significant difference in pore formation between the PLC-treated and
192 mock-treated cells (Figure 3D). This provides clear evidence that CD59 is not a receptor for
193 T3SS translocation, and additionally rules out any other GPI-linked protein for this potential
194 receptor role.

195

196 **CD59 is required for efficient focal adhesion disruption by *Yersinia***

197 Upon contact with host cells, the bacterial invasin and YadA proteins engage and activate
198 host β1-integrin receptors, leading to recruitment of signaling and cytoskeleton-binding proteins
199 such as paxillin, focal adhesion kinase (FAK), Src-family kinases, and p130Cas. These protein
200 complexes at the integrin cluster sites are called focal adhesions (33). Lipid raft domains are also
201 recruited and involved in integrin clustering and likely promote the assembly and reinforcement

202 of,focal adhesionts (FA)(34). *Yersinia* can disrupt these FAby translocating the YopH protein
203 tyrosine phosphatase, blocking phosphotyrosine signaling and the actin rearrangements that drive
204 phagocytosis (35-37). YopH has many host targets, including FAK, p130Cas, and Src-family
205 kinases at focal adhesion sites (33, 38, 39), as well as the tyrosine kinase Lck and the LAT
206 adapter in T cells (36, 40).

207 To determine whether CD59 activates focal adhesion formation as it does cytoskeletal
208 regulators in T cells (40), an anti-phosphotyrosine (pTyr) antibody was used to assess whether
209 reduced CD59 levels interfere with YopH tyrosine phosphatase activity during *Yptb* infection.
210 HeLa cells were knocked down with either siCD59 or the siNT control for 72 hours, challenged
211 with *Yptb gfp*$^{+}$ bacteria, fixed, and immunostained with anti-pTyr. Focal adhesions appear as
212 brightly stained fiber-like bundles, numerous in both siCD59 knockdown and siNT control cells
213 in the absence of infection (Figure 4A). In contrast, upon challenge with WT *Yersinia*, focal
214 adhesions were readily disassembled in CD59-positive siNT control cells, as evidenced by the
215 absence of large bundles and the increased number of puncta (Figure 4B, left panel). This
216 process was inefficient in the siCD59 knockdown cells, as larger focal adhesions were still
217 visible (Figure 4B, right panel) compared to the siNT control cells.

218 Focal adhesions were identified and measured by an image analysis routine that
219 distinguishes edges, based on a previously published workflow (41). The average size of each
220 focal adhesion and the total sum of pixels identified per cell were significantly lower in CD59-
221 positive control cells compared to the CD59 knockdown after bacterial infection (Figure 4C and
222 D, respectively), indicating that CD59 is required for efficient disruption of these host cell
223 signaling assemblies. This is consistent with a defect in YopH accumulation and/or targeting of
224 focal adhesions after bacterial contact with host cells deficient for CD59.

225

226 **Depletion of CD59 alters GM1 trafficking after *Yptb* challenge**

227 Our results indicate that the *Yptb* T3SS is highly sensitive to alterations in CD59 plasma
228 membrane content. CD59 is enriched in microdomains in the cell membrane where cholesterol,
229 glycosphingolipids, GPI-linked proteins, and signaling proteins are densely associated (24).
230 These receptor-rich microdomains are thought to be highly dynamic and may transiently
231 rearrange in response to activating signals, such as the adhesion of a pathogen (42). As CD59
232 plays an indirect role in supporting *Yptb*-dependent T3SS function (Figure 3), the dynamics of
233 host cell membrane organization were investigated as a function of CD59 expression, probing for
234 microdomains. Cholera toxin B subunit (CtxB) binds to the glycosphingolipid GM1 in lipid
235 microdomains and can be used to detect altered microdomain distribution in response to bacterial
236 binding (43). Therefore, the GM1 probe AlexaFluor594-CtxB was added to the cell culture
237 medium immediately before *Yptb* challenge of cells that had been siRNA-depleted of CD59 for
238 72 hr prior to infection, using nontargeting siRNA as the control (siCD59 and siNT respectively;
239 Materials and Methods).

240 In the absence of *Yptb* infection, GM1 was notably localized to the perinuclear region in
241 control CD59-positive cells (Figure 5A). After CD59 depletion, however, GM1 puncta
242 accumulate at the cell periphery when compared to the siNT control cells (compare Fig. 5A to
243 5B, two examples). When challenged with the T3SS-deficient *Yptb* ΔB mutant, there was largely
244 no change compared to the uninfected controls (compare Figs 5D to 5B). Strikingly, when siNT
245 cells were challenged with WT *Yptb*, any residual peripheral localization was largely lost and
246 GM1 was exclusively perinuclear (Figure 5E, two examples of tight perinuclear staining). In
247 stark contrast, infection of CD59 knockdown cells with WT *Yptb* resulted in total loss of

248 perinuclear localization and GM1 puncta dispersed across the whole cell surface (Figure 5F),
249 consistent with a defect in GM1 trafficking. Therefore, the absence of CD59 causes dispersion of
250 GM1 gangliosides in response to an intact T3SS. This phenotype was not due to alterations in
251 surface localization of GM1 gangliosides, as flow cytometry of cells probed for GM1 indicated
252 that CD59 knockdown had no effect on surface levels of GM1 compared to siNT control cells
253 (Figure S2). Diffuse punctate localization of GM1 and failure to coalesce perinuclearly are
254 therefore correlated with loss of CD59 and defects in supporting T3SS function.
255
256 **Loss of CD59 perturbs lipid composition of plasma membrane**
257 To investigate if the loss of CD59 results in changes of lipid composition, HEK 293T WT
258 and CD59-KO cells were extracted in 2:1 chloroform:methanol, and samples were analyzed by
259 LC-MS/MS to identify lipid components (44). Principal component analysis (PCA) of mass
260 spectrometry peak data normalized by percent abundance within each sample showed suitable
261 separation of samples by cell line (Figure 6A). The two most abundant lipid classes in both lines
262 were phosphatidylcholine (PC) and phosphatidylethanolamine (PE). The bulk sum carbon (C)
263 composition of the acyl chains for PC species detected by LC-MS/MS is shown in Figure 6B,
264 indicated by total number of carbons as a percentage sum of all PC lipids for each sample. Acyl
265 chain content species totaling 34 bulk sum carbons was by far the most abundant PC, and the
266 WT had significantly more of these species compared to CD59 KO cells ($P<0.05$). Interestingly,
267 the KO cells exhibited a greater number of lower (32 carbons) and very large acyl chain content
268 species (>40 bulk sum carbons) (Figure 6B). A similar trend was found in PE species (Figure
269 6C). WT cells had more of the most abundant 36C content species among PE, while greater

270 numbers of larger (38C) and smaller (<35C) species were detected in CD59KO cells compared
271 to WT cells (Figure 6C).
272 Sphingomyelin (SM) is enriched in ordered lipid raft domains and has been found to
273 preferentially organize with CD59 within the plasma membrane (45). Increased unsaturation of
274 SM results in greater area and decreased lateral diffusion rates of the lipid (46). There was a
275 significantly higher percentage of SM(36:2) (36 acyl carbons, 2 total double bonds) in CD59 KO
276 compared to WT cells (Figure 6D). The increased unsaturation within the SM 36C species may
277 result in less ordered membrane dynamics, potentially affecting lipid raft organization and ability
278 to coalesce in a perinuclear locale after bacterial contact (Figure 5). CD59 KO also altered flux
279 through several lipid biosynthesis and catabolic pathways, with similar directionality across two
280 independent experiments, as analyzed using the LIPIDMAPS BioPan software tool (Figure 6E)
281 (47). Altogether, these results indicate that the absence of CD59 alters the homeostatic
282 maintenance of lipid species composition in the host cell.
283
284 **Discussion**
285 In this work we demonstrated that optimal function of the *Yersinia pseudotuberculosis*
286 T3SS required host cell CD59. While depletion of host CD59 did not eliminate the ability of *Yptb*
287 to form pores and translocate effector Yop substrates into target cells, a marked reduction in
288 T3SS function was observed. This result indicates that CD59 is unlikely to function as a receptor
289 for the T3SS machinery. Consistent with an indirect role in supporting T3SS function, the release
290 of all surface-exposed GPI-linked proteins prior to infection did not reduce *Yptb*(Δ5)-dependent
291 pore formation. These data, together with the inability of the CD59-binding protein ILY^{PP} to

292 block the T3SS machinery, collectively indicate that CD59 is unlikely to directly interact with
293 pathogen components.

294 Host focal adhesion (FA) complexes are important signaling hubs targeted by the tyrosine
295 phosphatase YopH, which disassembles them and helps prevent phagocytosis of bacteria. We
296 found that CD59 facilitates efficient focal adhesion disruption by *Yptb* (Figure 4). In contrast,
297 CD59 depletion increased the average FA size, resulting in a greater total FA area per infected
298 cell. Since translocation is decreased in the absence of CD59, there may be less YopH available
299 to cause focal adhesion disassembly. Alternatively, CD59 has been shown to play a role in
300 several signal transduction pathways, including the activation of Src-family kinases such as Lyn,
301 Fyn, and Lck, some of which are known to interact with FAK (18, 40, 48). CD59 could be
302 involved in activating or recruiting these components to the site of bacterial binding, so that in its
303 absence, these pathways are muted or less accessible to the Yops. Lipid raft domains, of which
304 CD59 is a hallmark component, are also recruited and involved in integrin clustering and likely
305 promote the assembly and reinforcement of FAs (34). CD59 effects on trafficking may not be
306 limited to host cell components, as its loss may interfere with Yop localization, preventing access
307 to signaling structures normally targeted by the Yops.

308 A series of studies indicates that the T3SS translocation complex may interact with lipid
309 raft components. In our previous study, CCR5 was identified as important for T3SS function.
310 CCR5 is in the same family of G protein-coupled receptors (GPCRs) as Fpr1, a recently
311 identified receptor for *Yersinia pestis* that is not required for *Yptb* T3SS function (17, 49). That
312 CCR5 depletion did not completely abolish translocation of *Yptb* T3SS effectors is consistent
313 with *Yptb* targeting functionally redundant receptors, in contrast to the profound importance of
314 Fpr1 for *Y. pestis*. Interestingly, chemokine receptors are known to colocalize with membrane

315 raft markers such as GM1 (50). A similar T3SS-wielding pathogen, *Pseudomonas aeruginosa*,
316 was found to preferentially bind the host receptor glycosphingolipid globotriaosylceramide
317 (Gb3), and depletion of either flotillin or CD59, both found in raft nanodomains with Gb3,
318 reduced uptake of *P. aeruginosa* (51). Functional lipid rafts are important for adhesion and T3SS
319 function in *Shigella*, EPEC, and *Salmonella* as well (25-27). These findings indicate that the
320 organization of various host proteins into structured membrane regions may provide the most
321 efficient target for *Yersinia* to dock, form pores, and deliver Yops via the T3SS.

322 We examined whether CD59 affected ganglioside-rich domains by fluorescently labeling
323 the raft marker GM1. In uninfected cells, the GM1 marker was predominantly trafficked to the
324 perinuclear region in the presence of CD59. When CD59 was depleted, there were noticeably
325 more GM1 puncta visible around the cell periphery. This phenotype was markedly enhanced
326 upon infection with WT *Yptb.* Accumulation of the GM1 marker was only detected in the
327 perinuclear region in WT host cells, while this perinuclear localization was completely lost in the
328 absence of CD59 after contact with WT *Yptb*. CD59 may play a role in mobilization of GM1 to
329 the perinuclear region either through endocytosis, plasma membrane rearrangements, or
330 recycling of this marker back to the plasma membrane.

331 When CtxB binds GM1, it is internalized by receptor-mediated endocytosis, and
332 undergoes retrograde trafficking from the plasma membrane through the trans-Golgi network to
333 the ER. This is visualized as perinuclear localization, as we observed in cells with functional
334 CD59 (52). Internalization of GM1 from the surface results in sorting into recycling endosomes
335 followed by release back to the plasma membrane. The first step is visualized as formation of
336 puncta around the cytoplasm, followed by eventual accumulation in pericentriolar recycling
337 endosomes (53, 54). The absence of CD59 may shift how host endocytic pathways are utilized

338 after *Yptb* engagement, favoring a blockade after puncta formation. This could result from
339 changes in the plasma membrane that either prevent effective engagement of the T3SS
340 machinery, alter trafficking of bacterial effectors, or prevent hijacking of host factors by bacterial
341 effectors. Obviously, under CD59 depletion conditions, there must be some low-level or
342 improperly functioning activity of the T3SS that exacerbates the inability of the CtxB-engaged
343 GM1 to coalesce in a perinuclear locale in the absence of CD59.

344 The specific lipid composition of the host cell plasma membrane can affect its structure,
345 function, and interactions with pathogens. PC and PE are the two most abundant lipid classes. PC
346 is a cylindrical-shaped lipid that allows tight packing of lipids and is present in higher
347 concentrations along with sphingolipids in the outer leaflet of the plasma membrane (55, 56). PE
348 along with phosphatidylserine (PS) and phosphatidylinositol (PI) are mostly found in the inner
349 leaflet (56). Acyl chain length and degree of saturation are lipid characteristics known to affect
350 plasma membrane stability and fluidity (57). Longer acyl chains tend to increase saturation and
351 result in thicker membranes, which are also more resistant to bending (58). Within the PC lipid
352 species, acyl contents of 34C and 36C (34 and 36 total carbons in total acyl chain content) were
353 the most commonly detected acyl chain totals in our analysis. CD59 KO cells had fewer 34C and
354 36C total chain contents, while exhibiting an increase in longer total acyl chain content (>40)
355 compared to WT cells (Figure 6B). This same trend was observed among the PE lipid species:
356 CD59 KO cells had fewer 36C chain content species, which were most abundant in WT host
357 cells, but had increased very short and very long acyl chain contents compared to WT (Figure
358 6C).

359 Acyl chain saturation is also a determinant of plasma membrane organization and fluidity.
360 Fully unsaturated GM1 C16:0 species have been shown previously to co-cluster with CD59,

361 while C16:1 species did not (59). Our analysis showed that SM C36:2 acyl chains were increased
362 in CD59 KO cells compared to WT cells (Figure 6D). The increased levels of unsaturation could
363 have effects on membrane fluidity, raft formation, or lipid-protein interactions. BioPAN analysis
364 revealed altered flux through various catabolic and metabolic pathways, indicating that CD59 is
365 required for proper lipid homeostasis and plasma membrane maintenance (Figure 6E).
366 In this study we have shown that CD59 is required for efficient pore formation and
367 translocation of bacterial effectors via the *Yptb* T3SS. The depletion of CD59 revealed changes in
368 the localization of lipid raft marker GM1 indicating a largescale disruption of membrane
369 dynamics. CD59 is an important structural component of raft domains, and it is possible that
370 when cells lack this abundant GPI-linked protein, the formation, stability, and/or mobility of
371 these domains is disrupted. Disruption may result from deranged lipid signaling or from
372 preventing the interaction of T3SS components with host kinases involved in signal transduction.
373 Future work will focus on determining if other host components involved in lipid raft signaling
374 play critical roles in T3SS function, as well as on identifying the critical step in the T3SS
375 translocator insertion process that requires intact CD59.
376
377
378 **Materials and Methods**
379 **Bacterial Strains and Cell Culture Conditions.** All *Y. pseudotuberculosis* strains used
380 are derivatives of YPIII (wildtype) and were generously provided by Joan Mecsas (See Table 1).
381 HEK 293T cells (ATCC) and HeLa cells (ATCC) were maintained in Gibco DMEM + 10% fetal
382 bovine serum and incubated at 37°C, 5% CO_2.

383 **T3SS induction.** Single colonies of indicated *Yptb* strains were picked from agar plates
384 and grown in 2xYT broth overnight on a rotator at 26°C. Overnight cultures were diluted to A_{600}
385 = 0.200 in induction media (2xYT + 20mM $MgCl_2$ + 20mM $Na_2C_2O_4$), rotated at 26°C for 1.5
386 hours, then moved to 37°C and rotated for 1.5 hours to induce expression of the T3SS prior to all
387 infection assays.

388 **Generation of CRISPR CD59 knockout 293T cells.** Stable monoclonal CD59 KO
389 HEK 293T cells were generated using the LentiCRISPRv2 vector (a gift from Feng Zhang,
390 Addgene plasmid #52961) (28) targeting the 20bp sequence 5' ACGACGTCACAACCCGCTTG
391 3' of the human CD59 coding region. Oligonucleotides containing this targeted region plus 5'
392 BsmBI restriction sites (sense: CACCGACGACGTCACAACCCGCTTG and antisense:
393 AAACCAAGCGGGTTGTGACGTCGTC) were annealed and ligated into the LentiCRISPRv2
394 plasmid at the BsmBI digestion site. The sgRNA-containing vector was linearized within the
395 ampicillin cassette and transfected into WT 293T cells. After 48 hours transfected cells were
396 selected under puromycin and clonal populations were isolated, outgrown, and successful
397 knockout determined using fluorescent antibody labeling and FACS analysis as described below.
398 One knockout clone was used for all subsequent experiments, including the generation of clonal
399 cell lines with wildtype and high levels of CD59 surface expression.

400 **Generation of CD59 complement and overexpressing 293T cell lines.** 2 x 10^5 WT or
401 CD59 KO HEK 293T cells were seeded in 6-well tissue culture-treated plates and the pcDNA3.1
402 Hygro+ (empty vector) or pcDNA3.1 Hygro+ hCD59 plasmids were transfected using
403 Lipofectamine 2000 (Invitrogen). Hygromycin was added after 48 hours to select for transfected
404 cells, and transfectants were single-cell sorted into 96-well plates containing conditioned cell

405 media. Arising clonal populations were maintained with Hygromycin B to select against loss of
406 the integrated plasmid.

407 **Translocation Assay.** Approximately 2.5 x 10^5 HEK 293T cells were seeded in tissue
408 culture-treated 24 well dishes overnight. YPIII E-TEM or YPIIIΔ*yopB* E-TEM were grown in
409 induction conditions (See T3SS induction above), diluted in prewarmed DMEM including 10%
410 FBS, and added to 293T cells at an MOI = 1. The infection plates were centrifuged for 5 mins at
411 1000rpm to maximize bacterial contact with cells and incubated at 37°C, 5% CO_2, for 1 hr. Cells
412 were then harvested in 180 µl of PBS. A 10X solution of CCF4-AM reagents was prepared in
413 PBS (LiveBLAzer™ FRET - B/G Loading Kit with CCF4-AM, Invitrogen) (60), 20µL was
414 added to each sample tube, briefly vortexed, and incubated for 20 minutes protected from light at
415 room temperature. Samples were then analyzed on a BD FACS Calibur and data was processed
416 with FlowJo (Tree Star) software, with 10,000 events collected for each sample. Translocation
417 was quantified by subtracting background signal present in uninfected cells and calculating the
418 ratio of the geometric mean fluorescence intensity of the 450/515 channels.

419 **Pore Formation Assay.** Approximately 2.5 x 10^5 HEK 293T cells were seeded in tissue
420 culture-treated 24-well dishes overnight. Overnight bacterial cultures of YPIII Δ*yopHMOJE*
421 (YPIIIΔ5) or YPIIIΔ*yopB* (YPIIIΔB) were grown in T3SS induction conditions prior to infection
422 (See T3SS Induction). Induced YPIIIΔ*yopHMOJE* or YPIIIΔ*yopB* were diluted in prewarmed
423 DMEM + 10% FBS and added to HEK 293T cells at an MOI of 25. After challenge, plates were
424 centrifuged for 5 mins at 200xg and incubated at 37°C, 5% CO_2 for 2 hours. The contents of each
425 well were removed by pipetting the cells up and down, washing with Hanks' balanced salt
426 solution (HBSS), Gibco, resuspending in Live/Dead dye diluted 1:1000 in HBSS
427 (LIVE/DEAD™ Fixable Green Dead Cell Stain Kit, Molecular Probes, Life Technologies), and

428 incubated for 30 minutes protected from light. Cells were washed twice in HBSS containing 1%
429 Bovine Serum Albumin (BSA), resuspended in 0.300mL HBSS, and analyzed by flow cytometry
430 on a BD LSRII flow cytometer. At least 10,000 events were collected per sample. Pore formation
431 was quantified by determining the geometric mean of the FITC channel. Data was processed
432 with FlowJo (Tree Star) software.

433 **CD59 and GPI-linked surface protein detection.** Flow cytometry was utilized to
434 determine the levels of CD59 and GPI-linked proteins on the host cell surface. Live HEK 293Ts
435 cells were washed with PBS, blocked on ice in PBS containing 0.5% BSA for 10 minutes, and
436 pelleted for 5 mins at 300rcf. For CD59 detection, cells were resuspended in mouse anti-human
437 CD59-FITC (BD Pharminogen, clone p282 (H19)), diluted 1:500 in blocking buffer. To detect
438 GPI-linked proteins, cells were resuspended in fluorescently labeled proaerolysin (FLAER,
439 Alexa 488 variant, CedarLane Labs) diluted 1:20 in blocking buffer. Cells were incubated on ice
440 protected from light for 30 minutes, washed once in blocking buffer, resuspended, and
441 transferred to a round bottom polystyrene 12 x 75mm tube for flow cytometry analysis. When
442 fixation was required, cells were washed in PBS, fixed for 20 minutes in PBS containing 4%
443 paraformaldehyde (PFA) at RT, protected from light, washed 3x in PBS, blocked for 1hr in 4%
444 BSA, resuspended in either anti-CD59 or FLAER (1:500 or 1:20, respectively) for 1hr rotating at
445 37°C, washed once, resuspended in blocking buffer, then transferred to round bottom 5mL
446 polystyrene tubes for flow cytometry analysis.

447 **CD59 siRNA knockdown.** HEK 293T or HeLa cells were seeded in 6-well tissue
448 culture-treated plates overnight. 25pmol per well of siGENOME SMARTPOOL human CD59
449 siRNA (Horizon Discovery) or 25pmol of non-targeting control siRNA were transfected using
450 Lipofectamine RNAiMax (Invitrogen). After 48 hours, cells were lifted and seeded in 24-well

451 tissue culture plates. Cells were then challenged with induced YPIII strains after a total of 72
452 hours of siRNA knockdown.

453 **Phospholipase C Treatment.** 5.0 x 10^5 HEK 293T cells per well were seeded into 12-
454 well tissue culture-treated plates overnight. Overnight cultures of YPIII Δ*yopHMOJE* or
455 YPIIIΔ*yopB* were then diluted and induced (see T3SS induction). To cleave surface GPI-linked
456 proteins from HEK 293Ts cells, 0.1U of phospholipase C protein (Phosphatidylinositol-Specific
457 from *Bacillus cereus*, Invitrogen), or an equivalent volume of buffer was added to each well 30
458 minutes prior to infection and incubated at 37°C, 5% CO_2, then cells were infected at MOI = 25.
459 Plates were centrifuged for 5mins at 200xg and incubated at 37°C, 5% CO_2 for 2 hours.
460 Following infection, cells were either assayed for pore formation or probed with FLAER to
461 determine levels of GPI-linked proteins present on the host cell surface.

462 **Expression and purification of intermedilysin proteins.** Plasmid constructs for protein
463 expression of His-tagged WT intermedilysin (His-ILY^{WT}) and a prepore conformation mutant
464 (His-ILY^{PP}) were generously provided by Rodney K. Tweten (61). *E. coli* BL21 (DE3) cultures
465 harboring either the His-ILY^{WT} or His-ILY^{PP} plasmids were grown overnight in LB broth
466 supplemented with 100ug/mL carbenicillin. Overnight cultures were diluted 1:100 in LB and
467 incubated with agitation at 37°C until they reached an A_{600} = 0.8, supplemented with 100ug/mL
468 carbenicillin, and induced by adding 1mM IPTG (final concentration). Cultures were incubated
469 at room temperature overnight and pelleted at 5000rpm for 20 mins at 4°C. Pellets were
470 resuspended in 20mL PBS, 1x EDTA-free cOmplete Protease Inhibitor Cocktail (Sigma), cells
471 were lysed using a microfluidizer (Microfluidics), and the cell lysate centrifuged at 10,000rpm
472 for 30min at 4°C. Cleared lysates were applied to Ni-NTA resin, rotating end over end at 4°C for
473 1hr to allow adsorption, and mixture was transferred to a plastic column. After allowing flow-

474 through of the adsorption mix, the resin was washed with PBS containing steps of 0mM, 20mM,
475 50mM, 80mM, and 120mM imidazole, followed by elution of the protein with PBS containing
476 500mM imidazole, pH =7.2. Protein purity was determined by SDS-PAGE gel and Coomassie
477 staining, and protein concentrations were determined using Bradford reagent (Bio-Rad). Protein
478 was dialyzed overnight into 10mM MES (pH=6.5), 300mM NaCl, 1mM EDTA using dialysis
479 cassettes (Slide-a-Lyzer Cassettes, Thermo), then either stored short-term at 4°C, or long-term by
480 adding 10% glycerol and 5mM DTT before flash freezing for storage at -80°C.

481 **ILY Treatment.** Approximately 5 x 10^5 WT 293T cells were seeded overnight in 12 well
482 plates. To perform inhibitor experiments, cells were pretreated with 100nM ILY^{PP} or an
483 equivalent volume of buffer per well and incubated at 37°C, 5% CO_2 for 1 hr. After pretreatment,
484 cells were challenged with 30nM of ILY^{WT} or buffer, incubated for an additional 2 hours, and
485 assayed for pore formation (See Pore Formation Assay).

486 **Focal Adhesion Immunofluorescence Staining.** HeLa cells were seeded on glass
487 coverslips overnight in 24-well plates. Cells were wash and then challenged at MOI = 5,
488 centrifuged for 5 mins at 200xg, then immediately washed and fixed in 4% PFA. The fixed cells
489 were then washed with 0.05 M Tris buffered saline pH 8.0 (TBS) permeabilized in TBS
490 containing 0.1% Triton X-100 for 2-5 mins and blocked with TBS containing 1% BSA. Cells
491 were incubated with anti-phosphotyrosine, clone 4G10 (EMD Millipore) (1:200 in blocking
492 buffer), washed 3 times, and incubated with donkey anti-mouse IgG-Alexa-Fluor 594 (Jackson
493 ImmunoResearch Laboratories). Coverslips were stained with Hoechst, washed, and mounted
494 with ProLong Glass Antifade (Invitrogen). Images were taken with Zeiss AxioObserver.Z1
495 fluorescent microscope. Focal adhesions were identified and measured in ImageJ using a custom
496 macro that automates various functions to minimize background, increase contrast, and enhance

497 edge detection to identify focal adhesion particles, based on a previously published workflow
498 (41). See Supplementary materials for macro details.

499 **GM1 Immunofluorescence Staining.** HeLa cells were seeded overnight in DMEM
500 containing 10% fetal bovine serum on glass coverslips in 24-well plates. Prior to infection, the
501 culture medium was aspirated and fresh culture medium containing cholera toxin B (CtxB)
502 (Vybrant Lipid Raft Labeling Kit, Molecular Probes) was added. Cells were then infected at MOI
503 = 5 with *Yptb* diluted in DMEM + 10% FBS so that the final concentration of CtxB was 2μg/mL
504 in each well. Plates were placed in centrifuge, subjected to 5min spin at 200xg, then coverslips
505 were washed three times with cold medium, incubated with anti-CtxB at 4°C for 15mins, washed
506 three times with cold PBS, fixed in 4% PBS containing 4% PFA, washed three times in PBS,
507 stained with Hoechst (1:10000) and mounted with ProLong Glass Antifade (Invitrogen).

508 **Lipid Extraction and Data Analysis.** Lipids were extracted from WT and CD59 KO
509 293T cells by the Folch extraction method (44) as follows. CD59 KO and WT 293T cells were
510 grown in DMEM + 10% FBS until ~80% confluency in one 10cm plate per sample replicate, and
511 medium was changed 2 hours prior to harvesting. Cells were rinsed with PBS, lifted with 0.05%
512 trypsin, spun down for 5min at 200xg, washed with PBS, and resuspended with PBS in a total
513 volume of 200μL. Cells were transferred to glass vials and 2:1 chloroform: methanol was added
514 to a final volume of 4mL. Samples were then agitated for 30 min on an orbital shaker at RT
515 before 800μL water was added, vortexed 1 min, and allowed to stand for 10 minutes before
516 centrifuging for 5min at 1000xg to separate into three phases. The lower phase containing
517 nonpolar lipids was carefully transferred with a glass pipette from the vial into the microtube,
518 then evaporated under nitrogen and stored at -80 °C. Samples were then analyzed via high-
519 resolution LC-MS/MS, and the lipids were identified and quantified with LipidSearch software

by the BIDMC-Harvard Mass Spectrometry Facility according to their published protocol (special thanks to Dr. John Asara, Director) (44). Lipid peak data were normalized by percent abundance within each sample. PCA analysis was performed using MetaboAnalyst 5.0. Lipid pathway analysis performed using LIPIDMAPS BioPan software.

Acknowledgements

We would like to thank Dr. Rodney Tweten (Oklahoma University Health Science Center) for the kind gift of plasmids encoding intermedilysin derivatives and for discussions during the early stages of this work. We would like to thank Stephen Kwok and Alan Parmelee from the Tufts Flow Cytometry Core Facility for assistance in flow cytometry, Dr. Joan Mecsas and her lab for Yersinia strains and discussions, as well as Drs. Marta Gaglia and Katya Heldwein for experimental suggestions. We thank Drs. Efrat Hamami, Kevin Manera, Atish RoyChowdhury and Bixi He for critical review of the manuscript. This work was supported by NIAID awards R21AI085250, and R01AI110684 to R.R.I. KJD was supported by a NIAID Training Grant T32AI007422 and KLS was supported by NRSA postdoctoral fellowship F32 AI 082914-01 and Natalie V. Zucker Fellowship.

Author Contributions

Kristen Davis: conceptualized and designed the analysis, collected, analyzed, and interpreted the data, writing of original draft, editing of the paper; Kerri Sheahan: conceptualization, constructed CD59 KO cell line, collected preliminary data; Connor Murphy: conceptualization, collected preliminary data; Ralph Isberg: conceptualization and design of analysis, funding acquisition, project administration, methodology, interpretation of data, editing and review of manuscript.

545

546 **References**
547

548 1. Dewoody RS, Merritt PM, Marketon MM. 2013. Regulation of the Yersinia type III
549 secretion system: traffic control. Front Cell Infect Microbiol 3:4.
550 2. Cornelis GR. 2006. The type III secretion injectisome. Nat Rev Microbiol 4:811-25.
551 3. Bliska JB, Wang X, Viboud GI, Brodsky IE. 2013. Modulation of innate immune
552 responses by Yersinia type III secretion system translocators and effectors. Cell Microbiol
553 15:1622-31.
554 4. Cornelis GR, Boland A, Boyd AP, Geuijen C, Iriarte M, Neyt C, Sory MP, Stainier I.
555 1998. The virulence plasmid of Yersinia, an antihost genome. Microbiol Mol Biol Rev
556 62:1315-52.
557 5. Portnoy DA, Falkow S. 1981. Virulence-associated plasmids from Yersinia enterocolitica
558 and Yersinia pestis. J Bacteriol 148:877-83.
559 6. Gemski P, Lazere JR, Casey T, Wohlhieter JA. 1980. Presence of a virulence-associated
560 plasmid in Yersinia pseudotuberculosis. Infect Immun 28:1044-7.
561 7. Matteï PJ, Faudry E, Job V, Izoré T, Attree I, Dessen A. 2011. Membrane targeting and
562 pore formation by the type III secretion system translocon. FEBS J 278:414-26.
563 8. Viboud GI, Mejía E, Bliska JB. 2006. Comparison of YopE and YopT activities in
564 counteracting host signalling responses to Yersinia pseudotuberculosis infection. Cell
565 Microbiol 8:1504-15.
566 9. Aepfelbacher M, Trasak C, Wilharm G, Wiedemann A, Trulzsch K, Krauss K, Gierschik
567 P, Heesemann J. 2003. Characterization of YopT effects on Rho GTPases in Yersinia
568 enterocolitica-infected cells. J Biol Chem 278:33217-23.
569 10. Logsdon LK, Mecsas J. 2003. Requirement of the Yersinia pseudotuberculosis effectors
570 YopH and YopE in colonization and persistence in intestinal and lymph tissues. Infect
571 Immun 71:4595-607.
572 11. Black DS, Bliska JB. 2000. The RhoGAP activity of the Yersinia pseudotuberculosis
573 cytotoxin YopE is required for antiphagocytic function and virulence. Mol Microbiol
574 37:515-27.
575 12. von Pawel-Rammingen U, Telepnev M, Schmidt G, Aktories K, Wolf-Watz H, Rosqvist
576 R. 2000. GAP activity of the Yersinia YopE cytotoxin specifically targets the Rho
577 pathway: a mechanism for disruption of actin microfilament structure. Molecular
578 Microbiology 36:737-748.
579 13. Mejía E, Bliska JB, Viboud GI. 2008. Yersinia controls type III effector delivery into host
580 cells by modulating Rho activity. PLoS Pathog 4:e3.
581 14. Blondel CJ, Park JS, Hubbard TP, Pacheco AR, Kuehl CJ, Walsh MJ, Davis BM, Gewurz
582 BE, Doench JG, Waldor MK. 2016. CRISPR/Cas9 Screens Reveal Requirements for Host
583 Cell Sulfation and Fucosylation in Bacterial Type III Secretion System-Mediated
584 Cytotoxicity. Cell Host Microbe 20:226-37.
585 15. Deruelle V, Bouillot S, Job V, Taillebourg E, Fauvarque MO, Attree I, Huber P. 2021. The
586 bacterial toxin ExoU requires a host trafficking chaperone for transportation and to
587 induce necrosis. Nat Commun 12:4024.
588 16. Swimm AI, Kalman D. 2008. Cytosolic extract induces Tir translocation and pedestals in
589 EPEC-infected red blood cells. PLoS Pathog 4:e4.

590 17. Sheahan KL, Isberg RR. 2015. Identification of mammalian proteins that collaborate with
591 type III secretion system function: involvement of a chemokine receptor in supporting
592 translocon activity. MBio 6:e02023-14.
593 18. Kimberley FC, Sivasankar B, Paul Morgan B. 2007. Alternative roles for CD59. Mol
594 Immunol 44:73-81.
595 19. Sugita Y, Nakano Y, Tomita M. 1988. Isolation from human erythrocytes of a new
596 membrane protein which inhibits the formation of complement transmembrane channels.
597 J Biochem 104:633-7.
598 20. Holguin MH, Fredrick LR, Bernshaw NJ, Wilcox LA, Parker CJ. 1989. Isolation and
599 characterization of a membrane protein from normal human erythrocytes that inhibits
600 reactive lysis of the erythrocytes of paroxysmal nocturnal hemoglobinuria. J Clin Invest
601 84:7-17.
602 21. Rollins SA, Sims PJ. 1990. The complement-inhibitory activity of CD59 resides in its
603 capacity to block incorporation of C9 into membrane C5b-9. J Immunol 144:3478-83.
604 22. Giddings KS, Zhao J, Sims PJ, Tweten RK. 2004. Human CD59 is a receptor for the
605 cholesterol-dependent cytolysin intermedilysin. Nat Struct Mol Biol 11:1173-8.
606 23. Farrand AJ, Hotze EM, Sato TK, Wade KR, Wimley WC, Johnson AE, Tweten RK. 2015.
607 The Cholesterol-dependent Cytolysin Membrane-binding Interface Discriminates Lipid
608 Environments of Cholesterol to Support beta-Barrel Pore Insertion. J Biol Chem
609 290:17733-17744.
610 24. Simons K, Ehehalt R. 2002. Cholesterol, lipid rafts, and disease. J Clin Invest 110:597-
611 603.
612 25. Hayward RD, Cain RJ, McGhie EJ, Phillips N, Garner MJ, Koronakis V. 2005.
613 Cholesterol binding by the bacterial type III translocon is essential for virulence effector
614 delivery into mammalian cells. Mol Microbiol 56:590-603.
615 26. van der Goot FG, Tran van Nhieu G, Allaoui A, Sansonetti P, Lafont F. 2004. Rafts can
616 trigger contact-mediated secretion of bacterial effectors via a lipid-based mechanism. J
617 Biol Chem 279:47792-8.
618 27. Lafont F, van der Goot FG. 2005. Bacterial invasion via lipid rafts. Cell Microbiol 7:613-
619 20.
620 28. Sanjana NE, Shalem O, Zhang F. 2014. Improved vectors and genome-wide libraries for
621 CRISPR screening. Nat Methods 11:783-784.
622 29. Viboud GI, Bliska JB. 2005. Yersinia outer proteins: role in modulation of host cell
623 signaling responses and pathogenesis. Annu Rev Microbiol 59:69-89.
624 30. Harmon DE, Davis AJ, Castillo C, Mecsas J. 2010. Identification and characterization of
625 small-molecule inhibitors of Yop translocation in Yersinia pseudotuberculosis.
626 Antimicrob Agents Chemother 54:3241-54.
627 31. Soltani CE, Hotze EM, Johnson AE, Tweten RK. 2007. Specific protein-membrane
628 contacts are required for prepore and pore assembly by a cholesterol-dependent cytolysin.
629 J Biol Chem 282:15709-16.
630 32. Guignot J, Tran Van Nhieu G. 2016. Bacterial Control of Pores Induced by the Type III
631 Secretion System: Mind the Gap. Front Immunol 7:84.
632 33. Knodler LA, Celli J, Finlay BB. 2001. Pathogenic trickery: deception of host cell
633 processes. Nat Rev Mol Cell Biol 2:578-88.
634 34. Fuentes DE, Butler PJ. 2012. Coordinated Mechanosensitivity of Membrane Rafts and
635 Focal Adhesions. Cell Mol Bioeng 5:143-154.

636 35. Black DS, Montagna LG, Zitsmann S, Bliska JB. 1998. Identification of an amino-
637 terminal substrate-binding domain in the Yersinia tyrosine phosphatase that is required
638 for efficient recognition of focal adhesion targets. Mol Microbiol 29:1263-74.
639 36. Rolán HG, Durand EA, Mecsas J. 2013. Identifying Yersinia YopH-targeted signal
640 transduction pathways that impair neutrophil responses during in vivo murine infection.
641 Cell Host Microbe 14:306-17.
642 37. Andersson K, Carballeira N, Magnusson KE, Persson C, Stendahl O, Wolf-Watz H,
643 Fällman M. 1996. YopH of Yersinia pseudotuberculosis interrupts early phosphotyrosine
644 signalling associated with phagocytosis. Mol Microbiol 20:1057-69.
645 38. Persson C, Carballeira N, Wolf-Watz H, Fällman M. 1997. The PTPase YopH inhibits
646 uptake of Yersinia, tyrosine phosphorylation of p130Cas and FAK, and the associated
647 accumulation of these proteins in peripheral focal adhesions. EMBO J 16:2307-18.
648 39. Black DS, Bliska JB. 1997. Identification of p130Cas as a substrate of Yersinia YopH
649 (Yop51), a bacterial protein tyrosine phosphatase that translocates into mammalian cells
650 and targets focal adhesions. EMBO J 16:2730-44.
651 40. Lipp AM, Juhasz K, Paar C, Ogris C, Eckerstorfer P, Thuenauer R, Hesse J, Nimmervoll
652 B, Stockinger H, Schütz GJ, Bodenhofer U, Balogi Z, Sonnleitner A. 2014. Lck mediates
653 signal transmission from CD59 to the TCR/CD3 pathway in Jurkat T cells. PLoS One
654 9:e85934.
655 41. Horzum U, Ozdil B, Pesen-Okvur D. 2014. Step-by-step quantitative analysis of focal
656 adhesions. MethodsX 1:56-9.
657 42. Aigal S, Claudinon J, Romer W. 2015. Plasma membrane reorganization: A glycolipid
658 gateway for microbes. Biochim Biophys Acta 1853:858-71.
659 43. Klymchenko AS, Kreder R. 2014. Fluorescent probes for lipid rafts: from model
660 membranes to living cells. Chem Biol 21:97-113.
661 44. Breitkopf SB, Ricoult SJH, Yuan M, Xu Y, Peake DA, Manning BD, Asara JM. 2017. A
662 relative quantitative positive/negative ion switching method for untargeted lipidomics via
663 high resolution LC-MS/MS from any biological source. Metabolomics 13.
664 45. Kinoshita M, Suzuki KG, Matsumori N, Takada M, Ano H, Morigaki K, Abe M, Makino
665 A, Kobayashi T, Hirosawa KM, Fujiwara TK, Kusumi A, Murata M. 2017. Raft-based
666 sphingomyelin interactions revealed by new fluorescent sphingomyelin analogs. J Cell
667 Biol 216:1183-1204.
668 46. Niemela PS, Hyvonen MT, Vattulainen I. 2006. Influence of chain length and
669 unsaturation on sphingomyelin bilayers. Biophys J 90:851-63.
670 47. Gaud C, B CS, Nguyen A, Fedorova M, Ni Z, O'Donnell VB, Wakelam MJO, Andrews S,
671 Lopez-Clavijo AF. 2021. BioPAN: a web-based tool to explore mammalian lipidome
672 metabolic pathways on LIPID MAPS. F1000Res 10:4.
673 48. Wang LN, Gao MH, Wang B, Cong BB, Zhang SC. 2018. A role for GPI-CD59 in
674 promoting T-cell signal transduction via LAT. Oncol Lett 15:4873-4881.
675 49. Osei-Owusu P, Charlton TM, Kim HK, Missiakas D, Schneewind O. 2019. FPR1 is the
676 plague receptor on host immune cells. Nature 574:57-62.
677 50. Popik W, Alce TM, Au WC. 2002. Human immunodeficiency virus type 1 uses lipid raft-
678 colocalized CD4 and chemokine receptors for productive entry into CD4(+) T cells. J
679 Virol 76:4709-22.
680 51. Brandel A, Aigal S, Lagies S, Schlimpert M, Melendez AV, Xu M, Lehmann A, Hummel
681 D, Fisch D, Madl J, Eierhoff T, Kammerer B, Romer W. 2021. The Gb3-enriched

682 CD59/flotillin plasma membrane domain regulates host cell invasion by Pseudomonas
683 aeruginosa. Cell Mol Life Sci 78:3637-3656.
684 52. Chinnapen DJ, Chinnapen H, Saslowsky D, Lencer WI. 2007. Rafting with cholera toxin:
685 endocytosis and trafficking from plasma membrane to ER. FEMS Microbiol Lett
686 266:129-37.
687 53. Iglesias-Bartolome R, Trenchi A, Comin R, Moyano AL, Nores GA, Daniotti JL. 2009.
688 Differential endocytic trafficking of neuropathy-associated antibodies to GM1
689 ganglioside and cholera toxin in epithelial and neural cells. Biochim Biophys Acta
690 1788:2526-40.
691 54. Cai B, Xie S, Liu F, Simone LC, Caplan S, Qin X, Naslavsky N. 2014. Rapid degradation
692 of the complement regulator, CD59, by a novel inhibitor. J Biol Chem 289:12109-12125.
693 55. Torres M, Parets S, Fernandez-Diaz J, Beteta-Gobel R, Rodriguez-Lorca R, Roman R,
694 Llado V, Rossello CA, Fernandez-Garcia P, Escriba PV. 2021. Lipids in Pathophysiology
695 and Development of the Membrane Lipid Therapy: New Bioactive Lipids. Membranes
696 (Basel) 11.
697 56. Skotland T, Kavaliauskiene S, Sandvig K. 2020. The role of lipid species in membranes
698 and cancer-related changes. Cancer Metastasis Rev 39:343-360.
699 57. Vanni S, Riccardi L, Palermo G, De Vivo M. 2019. Structure and Dynamics of the Acyl
700 Chains in the Membrane Trafficking and Enzymatic Processing of Lipids. Acc Chem Res
701 52:3087-3096.
702 58. Rawicz W, Olbrich KC, McIntosh T, Needham D, Evans E. 2000. Effect of chain length
703 and unsaturation on elasticity of lipid bilayers. Biophys J 79:328-39.
704 59. Arumugam S, Schmieder S, Pezeshkian W, Becken U, Wunder C, Chinnapen D, Ipsen
705 JH, Kenworthy AK, Lencer W, Mayor S, Johannes L. 2021. Ceramide structure dictates
706 glycosphingolipid nanodomain assembly and function. Nat Commun 12:3675.
707 60. Nguyen GT, McCabe AL, Fasciano AC, Mecsas J. 2019. Detection of Cells Translocated
708 with Yersinia Yops in Infected Tissues Using β-Lactamase Fusions. Methods Mol Biol
709 2010:117-139.
710 61. LaChapelle S, Tweten RK, Hotze EM. 2009. Intermedilysin-receptor interactions during
711 assembly of the pore complex: assembly intermediates increase host cell susceptibility to
712 complement-mediated lysis. J Biol Chem 284:12719-26.
713 62. Maldonado-Arocho FJ, Green C, Fisher ML, Paczosa MK, Mecsas J. 2013. Adhesins and
714 host serum factors drive Yop translocation by yersinia into professional phagocytes
715 during animal infection. PLoS Pathog 9:e1003415.
716 63. Crimmins GT, Mohammadi S, Green ER, Bergman MA, Isberg RR, Mecsas J. 2012.
717 Identification of MrtAB, an ABC transporter specifically required for Yersinia
718 pseudotuberculosis to colonize the mesenteric lymph nodes. PLoS Pathog 8:e1002828.
719

720

721

Table 1 Bacterial strains used in this study		
Background	Strain	Reference
YPIII	YPIIIΔ*yopB* (YPIIIΔB)	(10)
YPIII	YPIIIΔ*yopHMOJE* (YPIIIΔ5)	(10)
YPIII	YPIII E-TEM	(62)
YPIII	YPIII *gfp*+	(63)
YPIII	YPIIIΔ*yopB gfp*+	(63)

722 **FIGURE LEGENDS**

723 **Figure 1. Knockout and increased surface levels of host cell CD59 result in inefficient pore**
724 **formation when challenged by *Yptb*.** (**A**) WT and CD59 KO HEK 293T cells were probed with
725 either FITC-conjugated α-human CD59 or isotype control and analyzed by flow cytometry to
726 quantitate cell surface CD59. Histogram displays total counts for fluorescence of FITC channel,
727 collecting 10,000 events per sample. **(B)** HEK 293T cells were challenged with
728 YPIIIΔ*yopHMOJE* (YPIIIΔ5) or YPIII*yopB* (YPIIIΔB) at MOI = 25 for 2 hours. Cells were
729 labeled with FITC LIVE/DEAD stain and analyzed by flow cytometry to determine extent of
730 pore formation (Materials and Methods). **(C)** CD59 KO 293T cells were transfected with a
731 plasmid expressing human CD59 and stable monoclonal cell lines were obtained with CD59
732 levels that were similar to endogenously expressed protein (WT1 and WT2) or which were
733 overexpressed (OE1 and OE2). The histogram indicates the level of FITC-conjugated α-human
734 CD59 labeling for the WT, CD59 KO, and pCD59 clones as determined by flow cytometry. **(D)**
735 Indicated cell lines were challenged at MOI = 25 for 2 hrs with YPIIIΔ5 (See Supplemental
736 Figure S1 for YPIIIΔB control). Cells were labeled with FITC LIVE/DEAD stain and analyzed
737 by flow cytometry to determine extent of pore formation. Data are geometric mean ± SEM of the
738 fluorescence intensity normalized to WT. Results represent three independent experiments
739 performed in technical triplicate. Statistical significance was calculated using a one-way ANOVA
740 with Dunnett's multiple comparison test (*$p < 0.05$).

741

742

743 **Figure 2. Knockdown of host cell CD59 inhibits translocation of T3SS substrates during**

744 ***Yptb* infection.** WT 293T cells were transfected with either human CD59 siRNA or non-

745 targeting control siRNA to knock down CD59 expression. Assays were performed after 72 total

746 hours of transfection. **(A)** Cells were probed with FITC-conjugated α-human CD59 and analyzed

747 by flow cytometry for cell surface localization of CD59. **(B, C)** Approximately 2.5 x 10^5 siRNA

748 transfected cells were seeded overnight. Cells were challenged with YPIII/YopE-TEM or

749 YPIIIΔ*yopB*/YopE-TEM at MOI = 1 for 1 hour. Infected cells were harvested, loaded with

750 CCF4-AM and analyzed by flow cytometry. **(B)** Contour plots displaying the fluorescence

751 intensity of the blue channel (450nm), indicative of YopE translocation, vs. the green channel

752 (515nm) displaying all cells. **(C)** Translocation was calculated as the geometric MFI ratio for the

753 450/515 channels. Data shown are a representative experiment (from 3 independent experiments

754 performed in technical triplicate). Not significant: ns; $p<0.0001$: ****; $p<0.05$: *.

755

756 **Figure 3. Host cell CD59 indirectly supports YPIII T3SS-dependent pore formation. (A,B)**

757 ILY^{PP} treatment effectively blocks binding and subsequent pore formation by ILY^{WT}. WT 293T

758 cells were seeded overnight in 12-well plates. Cells were pretreated with 100nM of ILY^{PP} or

759 buffer for 1 hour, challenged with either 30nM ILY^{WT} **(A)** or YPIIIΔ5 or YPIIIΔB at MOI=25 **(B)**

760 and incubated for 2 hours. Cells were harvested and assayed for pore formation. Results shown

761 in panels A and B represent the mean from three independent experiments in technical duplicate

762 or triplicate, and all pore formation data were normalized to untreated 293T cells challenged by

763 YPIIIΔ5. **(C)** WT HEK 293T cells were seeded overnight in 12-well plates. Cells were treated

764 with phospholipase C (PLC) and incubated at 37°C, 5% CO_2 for 30 mins before harvesting and

765 labeling with FLAER for detection of GPI-linked proteins by flow cytometry. **(D)** WT HEK
766 293T cells were seeded overnight in 12-well plates and pretreated with PLC or buffer prior to
767 challenge with YPIIIΔ5 or YPIIIΔB at MOI = 25 for 2 hrs. Cells were then harvested and
768 assayed for pore formation. Data are geometric means ± SEM of MFI after subtraction of
769 uninfected control cell background and normalized to untreated 293T cells challenged by
770 YPIIIΔ5. Results represent three independent experiments done in technical duplicate or
771 triplicate. Statistical significance was calculated using an unpaired two-tailed Welch's t test (*p <
772 0.05).
773
774 **Figure 4. CD59 depletion lowers focal adhesion disruption by *Yptb*.** HeLa cells were
775 transfected with either siCD59 or the siNT control for 72 hours. Cells were challenged with *Yptb*
776 *gfp*+ at an MOI = 5 by 5 min centrifugation at 200xg followed by immediate washing and fixing.
777 The cells were then immunostained with anti-a followed by probing with anti-mouse-AF594, and
778 nuclei were stained with Hoechst (1:10000). **(A)** Focal adhesion staining with anti-pTyr of
779 uninfected cells. **(B)** Cells challenged with *Yptb gfp*+. Scale bar = 10μm. Focal adhesions were
780 identified and measured as described (Materials and Methods). **(C, D)** Average size and total area
781 displayed. Data analyzed using Ordinary One Way ANOVA followed by Sidak's test (*p < 0.05).
782
783 **Figure 5. CD59 knockdown affects localization of the lipid raft marker GM1.** HeLa cells
784 were transfected for 72 hrs with 25nM of siCD59 or non-targeting siRNA, then seeded on glass
785 coverslips for 24hrs prior to bacterial challenge. **(A, B)** Uninfected. **(C,D)** Cells challenged with
786 YPIIIΔB(pGFP). **(E,F)** Cells challenged with YPIII-WT(pGFP). Infections were performed at
787 MOI = 5 in presence of CtxB-AlexaFluor594. Bacterial-host cell contact was initiated by 5 min

788 centrifugation at 200xg followed by immediate washing and incubation with α-Ctx. Cells were
789 fixed with 4% PFA, and nuclei stained with Hoechst (1:10000). Scale bar = 10μm
790
791 **Figure 6. CD59 KO alters cellular lipid composition.** Lipids were extracted from HEK 293T
792 WT and CD59 KO cells (Materials and Methods). Representative results of two independent
793 experiments performed in triplicate. **(A)** Knockout of CD59 alters lipid profile. Principal
794 component analysis (PCA) of CD59 KO vs WT cells. Data was normalized by percent
795 abundance within each sample. **(B)** Sum of carbon counts of PC acyl species as a percentage of
796 total PC within each sample. **(C)** Sum of carbon counts of PE acyl species as a percentage of
797 total PE within each sample. **(D)** Saturation levels of SM lipid species as a percentage of total
798 SM within each sample. Significance determined by unpaired t test using two-stage step-up with
799 FDR of 1% for multiple comparisons. **(E)** Alteration of lipid flux as a consequence of loss of
800 CD59. Lipid peak data normalized by percent abundance was analyzed using LIPIDMAPS
801 BioPan software, available through LIPIDMAPS.org (47). Lipid subclass pathways displayed
802 were found to be similarly altered in both experiments.
803
804 **Figure S1. Pore formation by *Yptb* is T3SS-dependent.** CD59KO HEK 293T cells were
805 transfected with a plasmid expressing human CD59, and stable monoclonal cell lines were
806 obtained with CD59 levels that were similar to endogenously expressed protein (WT1 and WT2)
807 or which were overexpressed (OE1 and OE2). Indicated cell lines were challenged with
808 YPIIIΔ*yopHMOJE* (YPIIIΔ5) or YPIIIΔ*yopB* (YPIIIΔB) at MOI = 25 for 2 hrs. Cells were
809 labeled with FITC LIVE/DEAD stain and analyzed by flow cytometry to determine extent of

810 pore formation. Data are geometric mean ± SEM of the fluorescence intensity normalized to WT.

811 Data shown is representative of three individual experiments.

812

813 **Figure S2.** CD59 knockdown does not change surface levels of GM. **(A, B)** siNT control cells

814 and siCD59 knockdown cells were probed with FITC-conjugated α-human CD59 **(A)** or

815 immunolabeled for GM1 **(B)** and analyzed by flow cytometry after a 72 hr knockdown.

816

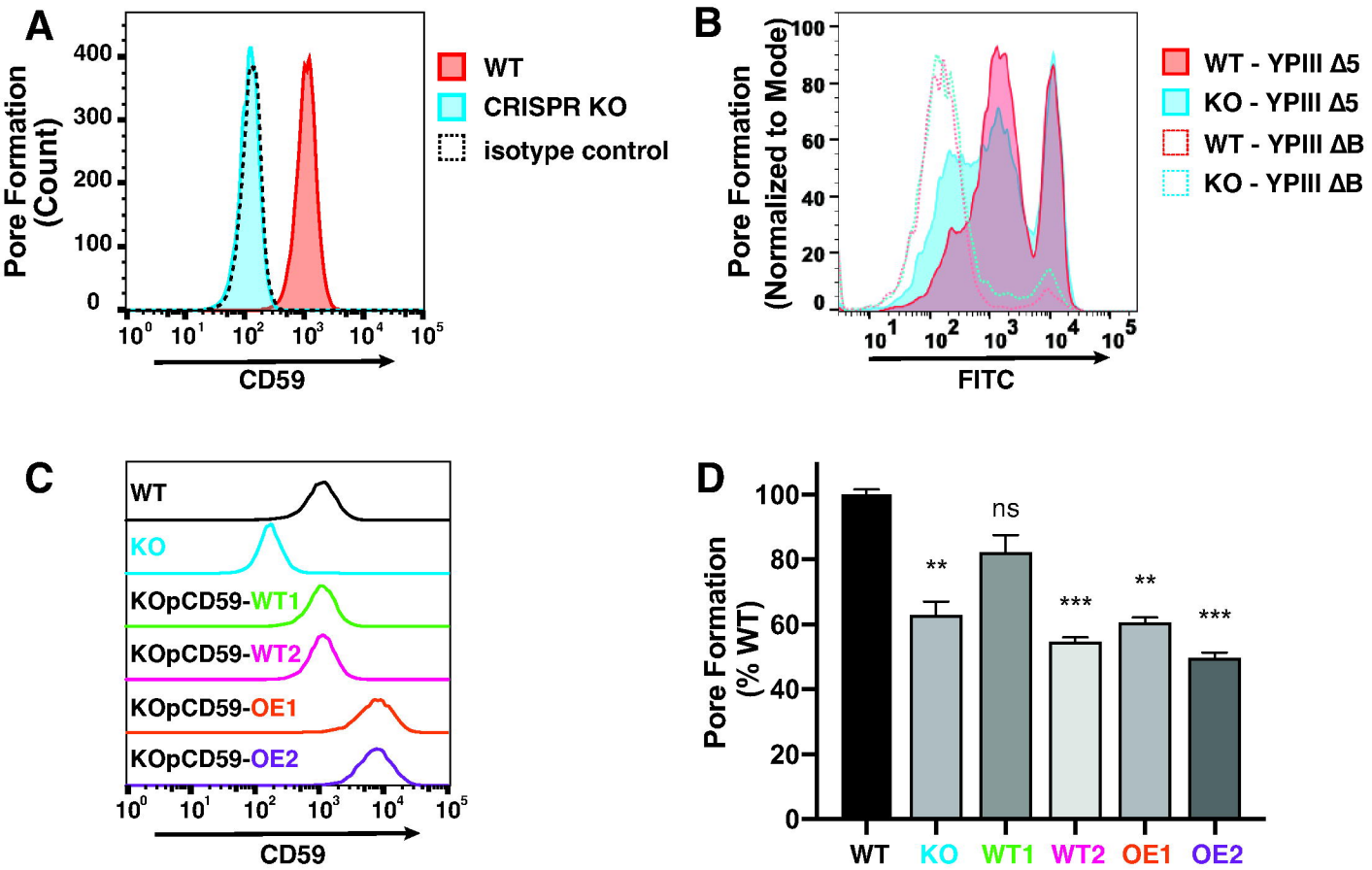
A
Pore Formation (Count)
400
300
200
100
0
10^0 10^1 10^2 10^3 10^4 10^5
CD59
WT
CRISPR KO
isotype control
B
Pore Formation (Normalized to Mode)
100
80
60
40
20
0
10^1 10^2 10^3 10^4 10^5
FITC
WT - YPIII Δ5
KO - YPIII Δ5
WT - YPIII ΔB
KO - YPIII ΔB
C
WT
KO
KOpCD59-WT1
KOpCD59-WT2
KOpCD59-OE1
KOpCD59-OE2
10^0 10^1 10^2 10^3 10^4 10^5
CD59
D
Pore Formation (% WT)
100
80
60
40
20
0
ns
**
***
**
***
WT
KO
WT1
WT2
OE1
OE2

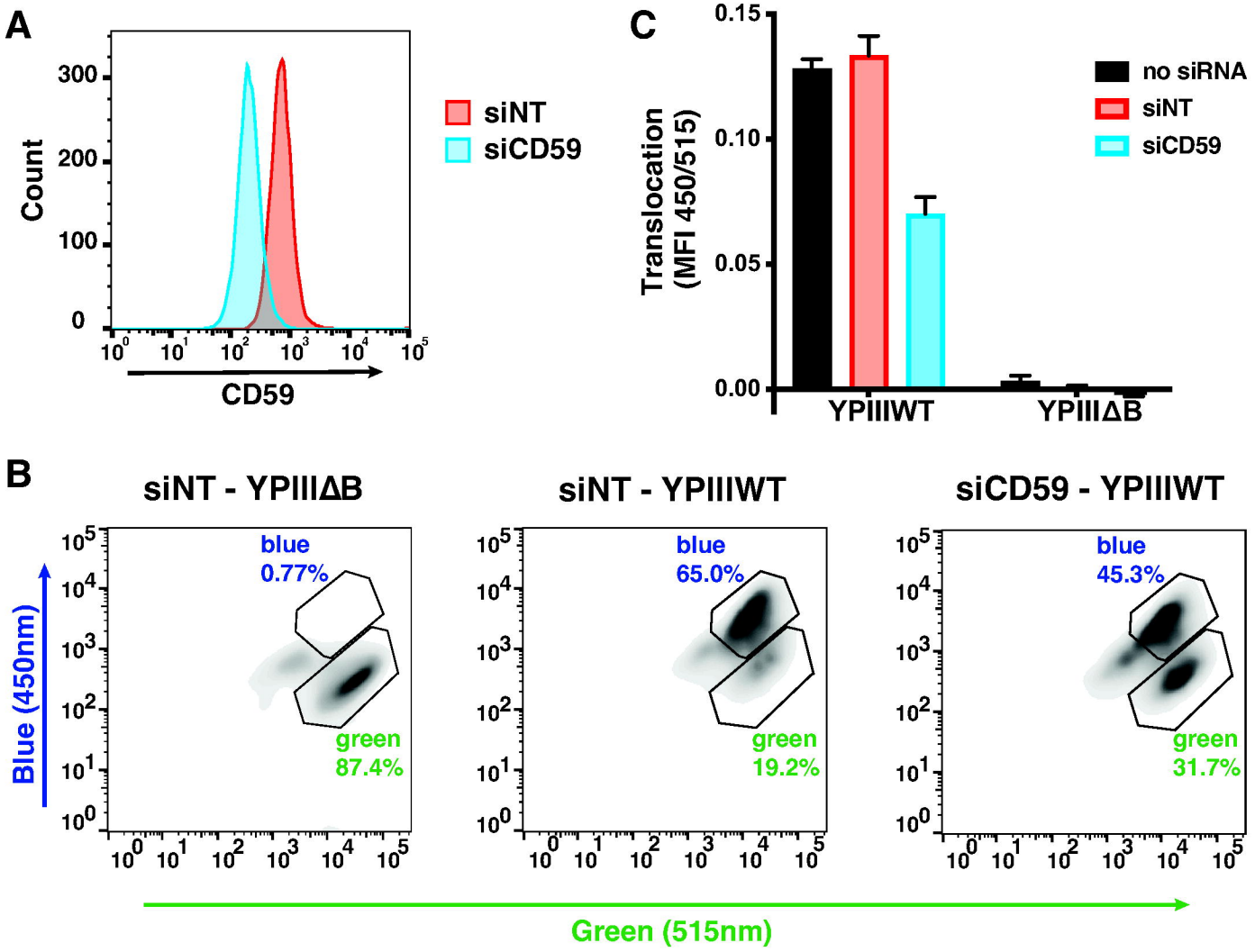
A
Count
300
200
100
0
CD59
siNT
siCD59
C
Translocation (MFI 450/515)
0.15
0.10
0.05
0.00
no siRNA
siNT
siCD59
YPIIIWT
YPIIIΔB
B
siNT - YPIIIΔB
siNT - YPIIIWT
siCD59 - YPIIIWT
blue
0.77%
green
87.4%
blue
65.0%
green
19.2%
blue
45.3%
green
31.7%
Blue (450nm)
Green (515nm)

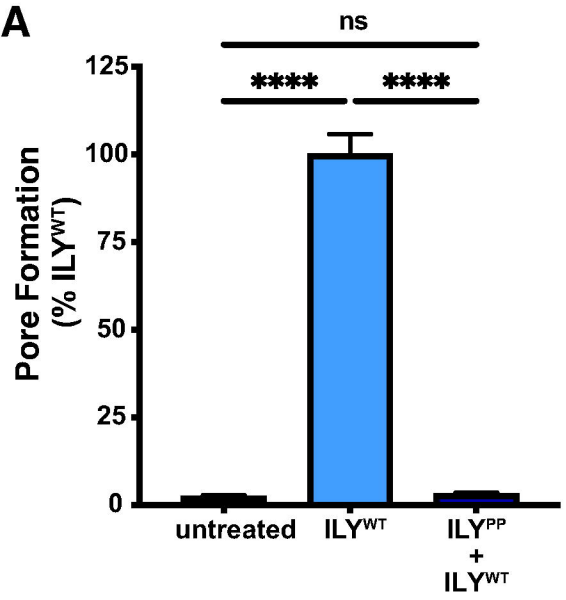
A
ns
****
****
125
100
75
50
25
0
Pore Formation
(% ILY^WT)
untreated
ILY^WT
ILY^PP
+
ILY^WT

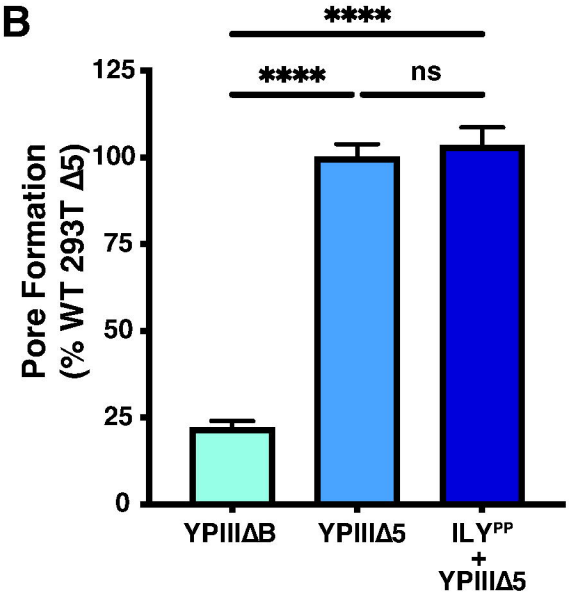
B
****
****
ns
125
100
75
50
25
0
Pore Formation
(% WT 293T Δ5)
YPIIIΔB
YPIIIΔ5
ILY^PP
+
YPIIIΔ5

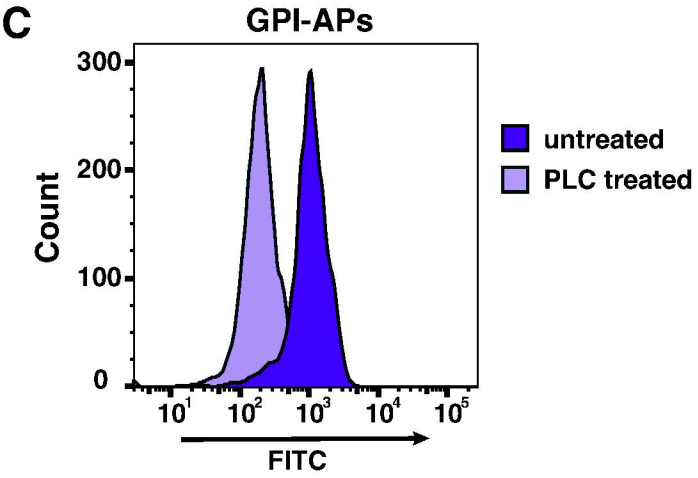
C
GPI-APs
300
200
100
0
Count
10^1
10^2
10^3
10^4
10^5
FITC
untreated
PLC treated

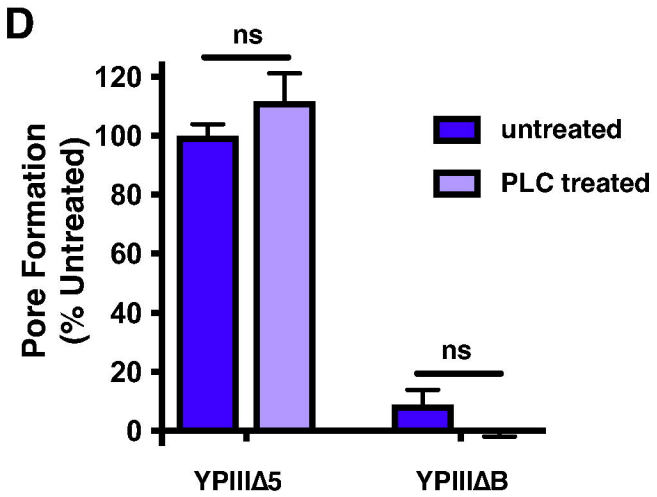
D
ns
ns
120
100
80
60
40
20
0
Pore Formation
(% Untreated)
untreated
PLC treated
YPIIIΔ5
YPIIIΔB

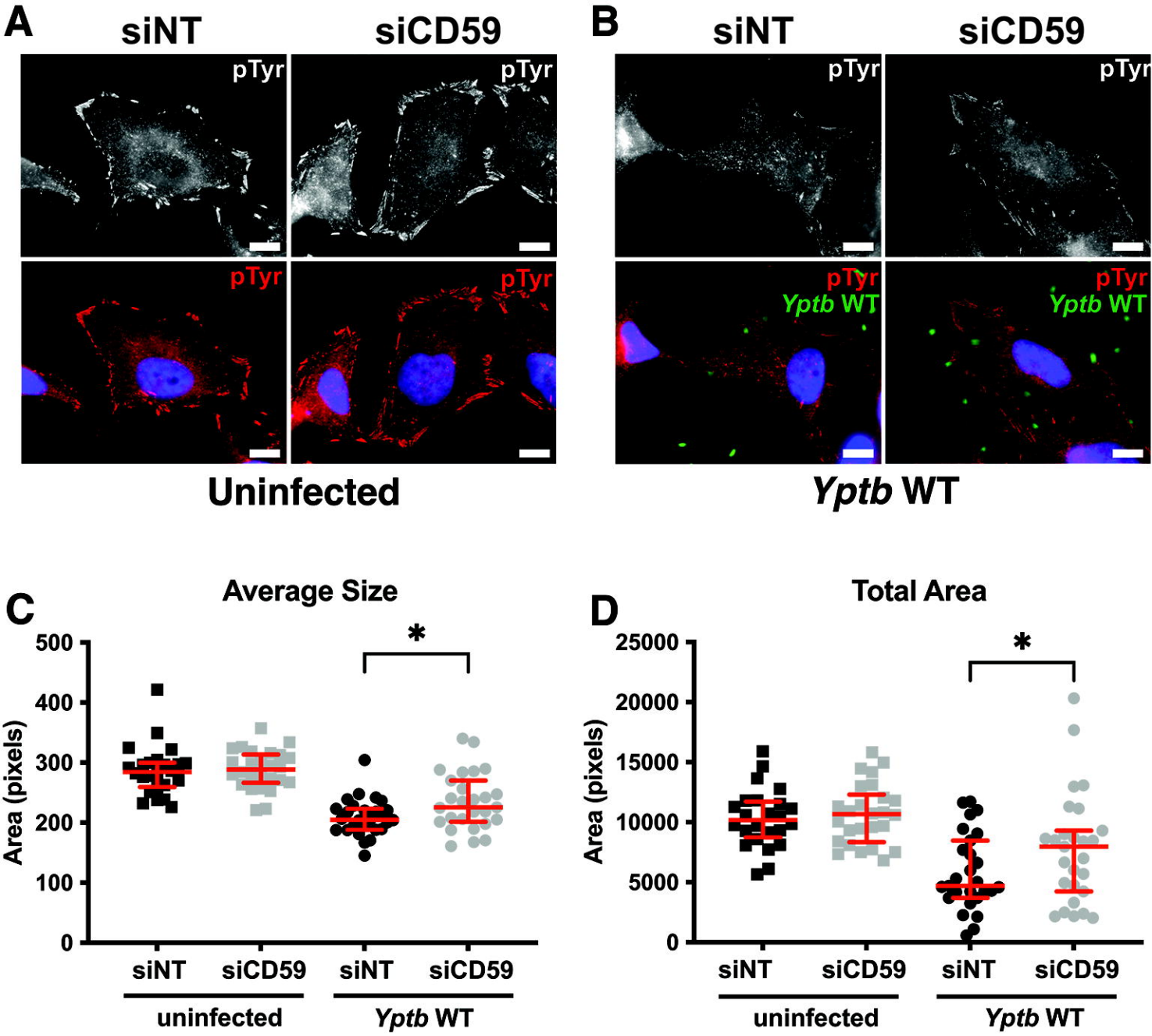
A
siNT
siCD59
pTyr
pTyr
pTyr
pTyr
Uninfected
B
siNT
siCD59
pTyr
pTyr
pTyr
Yptb WT
pTyr
Yptb WT
Yptb WT
C
Average Size
Area (pixels)
500
400
300
200
100
0
*
siNT
siCD59
siNT
siCD59
uninfected
Yptb WT
D
Total Area
Area (pixels)
25000
20000
15000
10000
5000
0
*
siNT
siCD59
siNT
siCD59
uninfected
Yptb WT

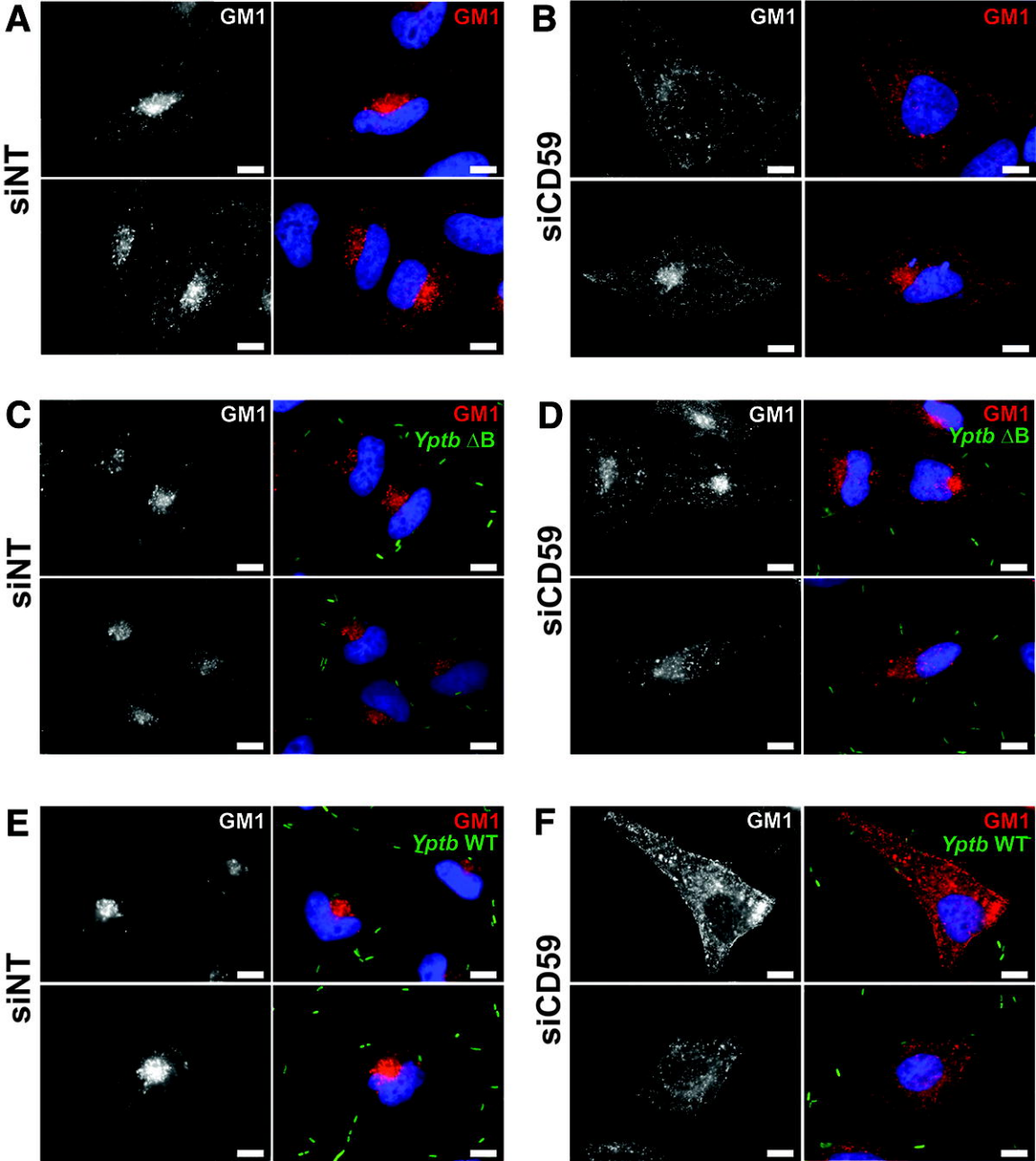
A
GM1
GM1
siNT
B
GM1
GM1
siCD59
C
GM1
GM1
Yptb ΔB
siNT
D
GM1
GM1
Yptb ΔB
siCD59
E
GM1
GM1
Yptb WT
siNT
F
GM1
GM1
Yptb WT
siCD59

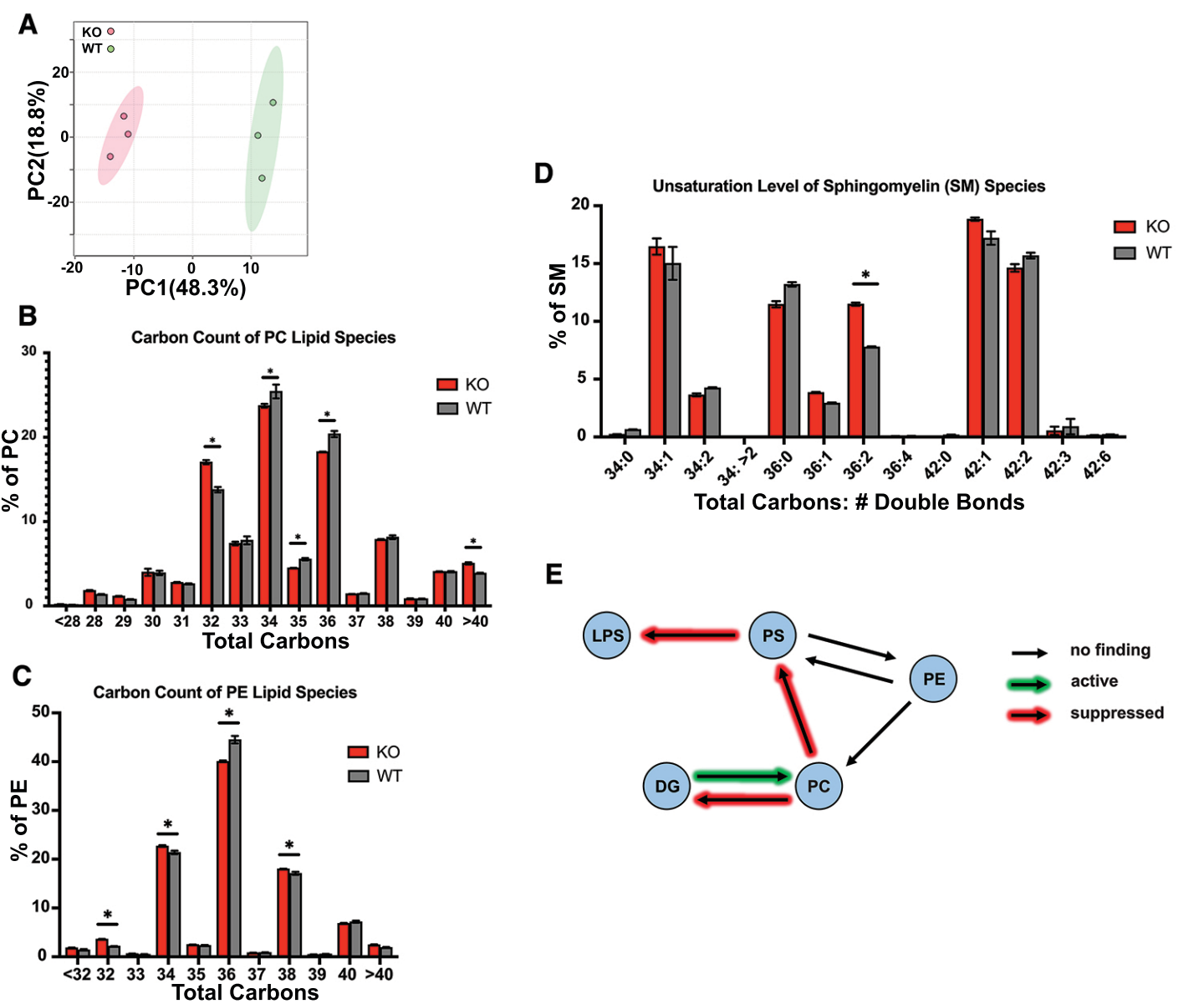
A
KO
WT
PC2(18.8%)
PC1(48.3%)
B
Carbon Count of PC Lipid Species
% of PC
KO
WT
<28 28 29 30 31 32 33 34 35 36 37 38 39 40 >40
Total Carbons
C
Carbon Count of PE Lipid Species
% of PE
KO
WT
<32 32 33 34 35 36 37 38 39 40 >40
Total Carbons
D
Unsaturation Level of Sphingomyelin (SM) Species
% of SM
KO
WT
34:0 34:1 34:2 34: >2 36:0 36:1 36:2 36:4 42:0 42:1 42:2 42:3 42:6
Total Carbons: # Double Bonds
E
LPS
PS
PE
DG
PC
no finding
active
suppressed

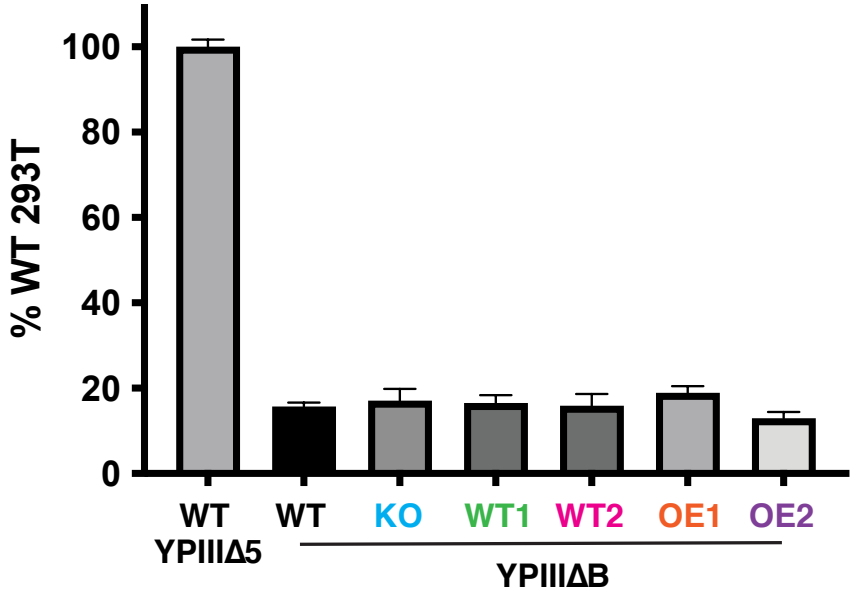

Figure S1. Pore formation by *Yptb* is T3SS-dependent

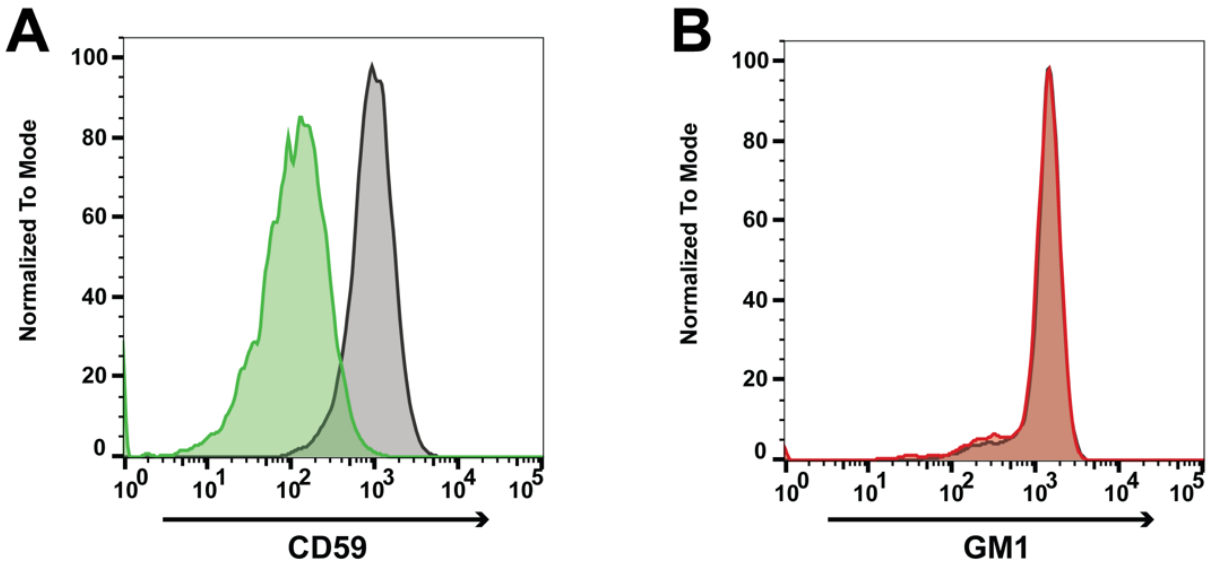

Figure S2. CD59 knockdown does not change surface levels of GM1